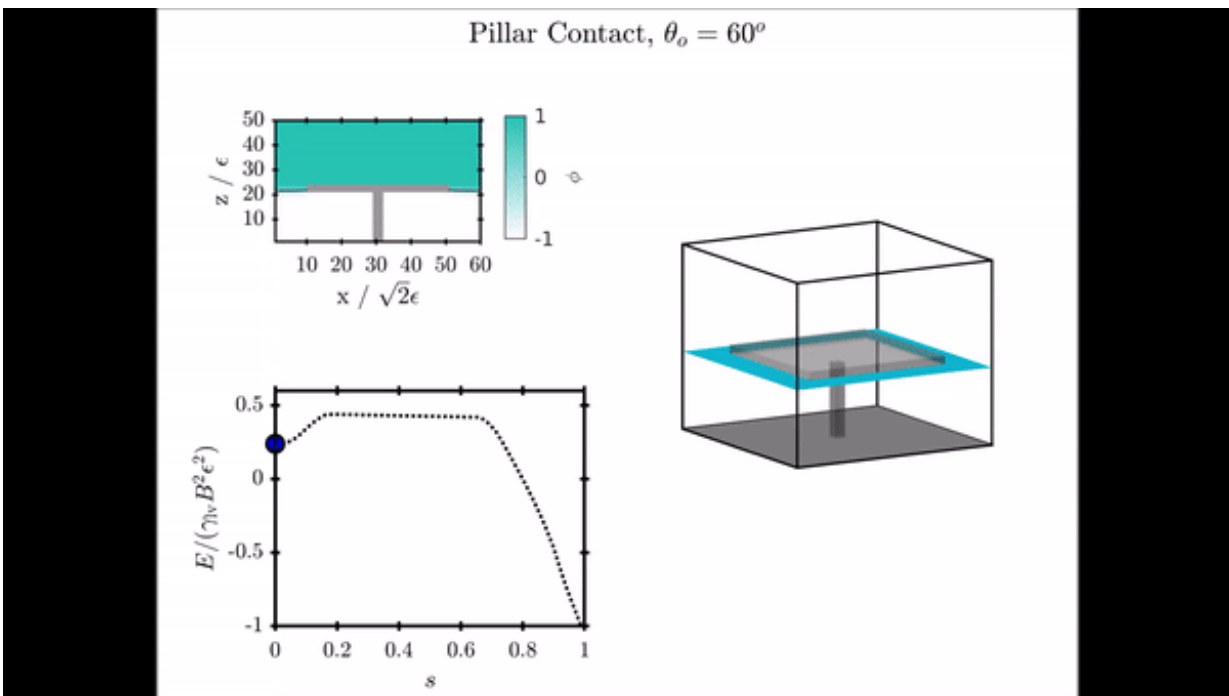


# Multifaceted design optimization for superomniphobic surfaces

June 28 2019, by Thamarasee Jeewandara



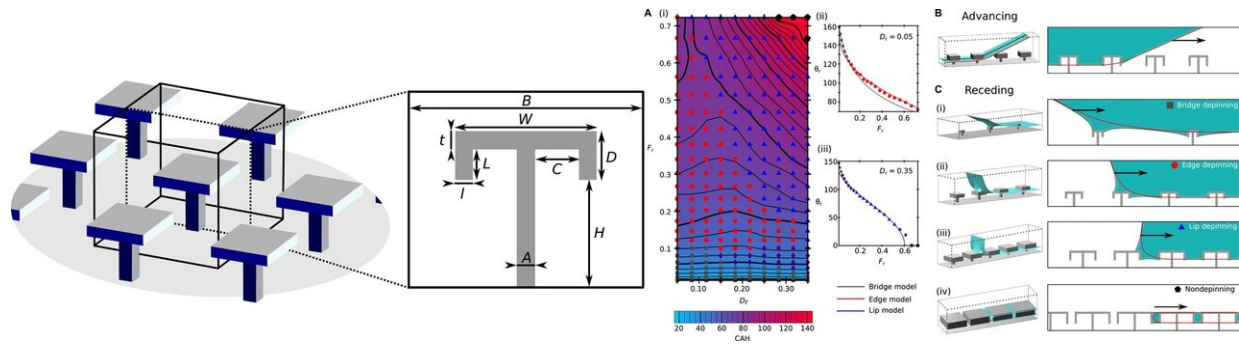
Video shows the pillar contact (PC) mechanism for a doubly reentrant geometry at  $\theta^\circ = 60^\circ$  a surface property identified in the study. Credit: Science Advances, doi: 10.1126/sciadv.aav7328

In [materials science](#), surfaces that strongly repel low surface tension liquids are classified 'superoleophobic,' while high surface tension liquid repellants are 'superhydrophobic' and surfaces that display both characteristics are 'superomniphobic.' Superomniphobic surfaces are at

the frontiers of surface design for a vast array of applications. In a recent study, J. R. Panter and co-workers at the Department of Physics and Procter and Gamble Co. in the U.K. and the U.S. developed computational methods to systematically develop three key surface wetting properties. These included contact angle hysteresis, critical pressure and a minimum energy wetting barrier. In the study, the scientists developed quantitative models and corrected inaccurate assumptions within existing models.

Panter et al. combined these analyses simultaneously to demonstrate the power of the strategy to optimize structures for applications in membrane distillation and digital microfluidics. By antagonistically coupling the wetting properties, the scientists implemented a multifaceted approach to optimally design superomniphobic surfaces. Using [genetic algorithms](#), they facilitated efficient optimization for speedups of up to 10,000 times. The results of the study are now published on *Science Advances*.

Superomniphobic surfaces have physical micro- and nanotextures that allow low-surface-tension liquids (oils and alcohols) to remain suspended on a vapor-filled surface structure. This liquid-shedding ability can promote [efficient droplet mobility with low viscous drag](#), with transformative potential across a broad range of applications. These include [sustainable technologies for water purification](#), [antimicrobial strategies](#) in biomedicine, [anti-fingerprint coating](#) techniques, [reducing food waste](#) and versatile [biochemical technologies](#), at the global scale.

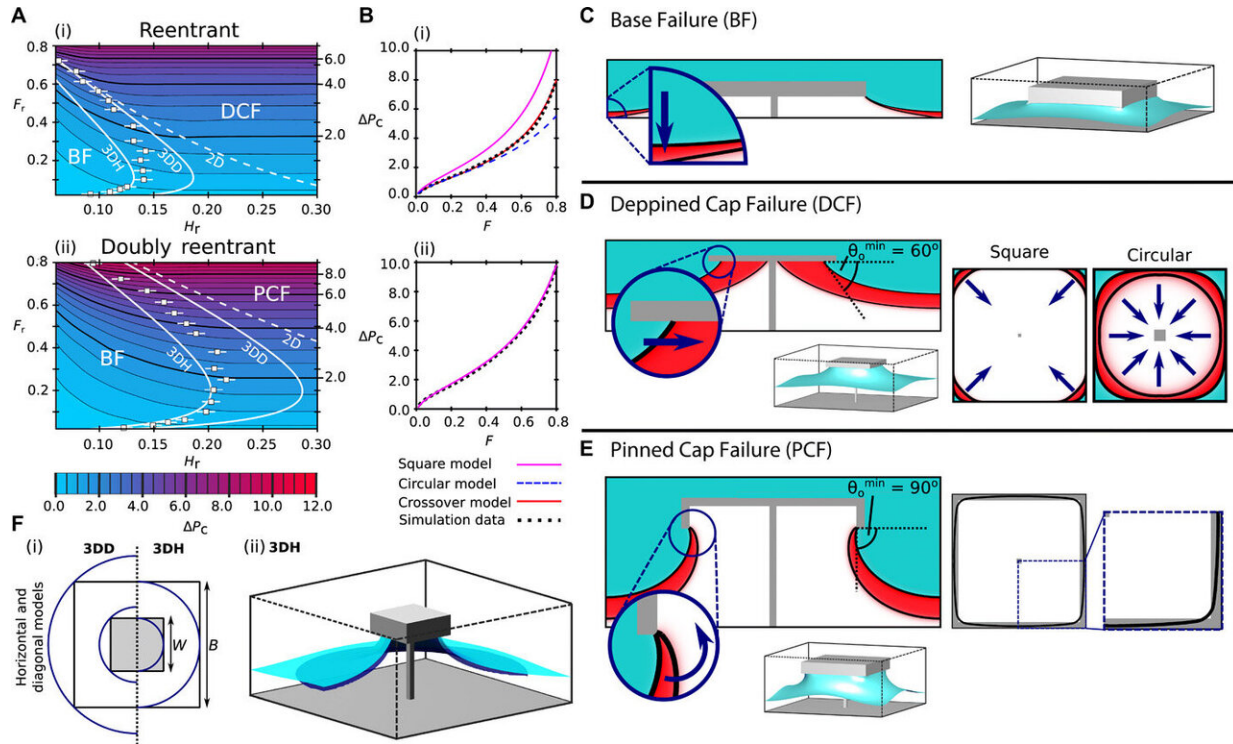


LEFT: Simulation surface configuration. Illustration of the 3D simulation repeat unit, with 2D cross section showing labeled structural parameters. RIGHT: Quantification and mechanisms leading to the CAH (contact angle hysteresis) for reentrant and doubly reentrant geometries at zero applied pressure. (A) (i) CAH dependence on both the area fraction  $F_r$  and total cap height  $D_r$ . Symbols indicate the depinning mechanism upon receding, with purple diamonds indicating a hybrid mechanism. (ii and iii) Comparison of the bridge-, edge-, and lip-depinning receding models (solid lines, color-coded) against the simulated  $\theta_r$  (data points); examples shown with varying  $F_r$  at fixed  $D_r = 0.05$  and  $0.35$ . The  $\pm 1^\circ$  error bars in the simulation data are too small to be seen. (B) 3D visualization of the advancing liquid-vapor interface (shown in blue); the advancing direction is indicated by a black arrow. Black and red lines indicate the center and edge 2D cross sections that are also presented (right). (C) (i to iv) Visualizations of the major four receding mechanisms. The receding direction is indicated by black arrows. Credit: Science Advances, doi: 10.1126/sciadv.aav7328

Recent breakthroughs in microfabrication have allowed the formation of complex structures at the micrometer scale resolution, including [three-dimensional \(3-D\) printing](#) technology, fluidization of polymer micropillars and [lithographic methods](#). Despite these highly versatile techniques, materials scientists and physicists still seek to understand how to precisely design surface structures for optimal performance in real-world applications. A successful omniphobic design must

demonstrate three key wetting properties to include (1) a [low contact angle](#) for maximum liquid mobility, (2) [high critical pressure](#) for stability of the superoleophobic state, and (3) a high [energetic barrier](#) to failure. Due to complexities of surface design, uniting computational and experimental studies can be expensive and time-consuming to understand this basis.

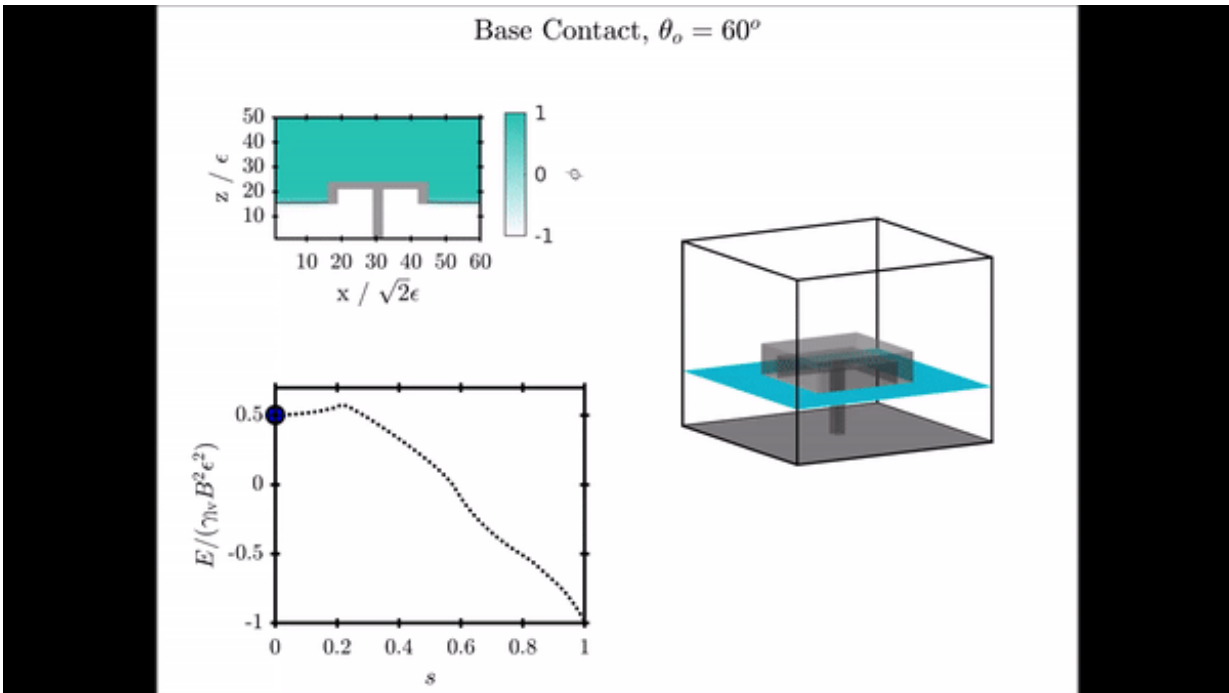
In the present work, Panter et al. overcame the challenges of designing superomniphobic wetting properties by first designing computational strategies to understand the effect that structural parameters had on the three defined criteria. To illustrate the importance of multifaceted optimization they used two relevant examples of [water purification](#) via membrane distillation and droplet-based digital microfluidics. The scientists developed a genetic algorithm to efficiently perform simultaneous optimizations with speedup to 10,000 times. This versatile approach can be coupled to [recent innovations in complex surface microfabrication](#) techniques to offer a transformative approach to surface design.



Critical pressure analysis for reentrant and doubly reentrant geometries. (A) Contour plots of  $\Delta P_c$  variation with  $F_r$  and  $H_r$  for reentrant (i) and doubly reentrant (ii) geometries. Data points mark the critical height at which the failure mechanism switches from Base Failure (BF) to Depinned Cap Failure (DCF) or Pinned Cap Failure (PCF), and error bars indicate the uncertainty in this height due to the diffuse interface width. Solid and dashed white lines show the critical height based on the capillary model and 2D model, respectively. (B) Model fits to  $\Delta P_c$  of the Cap Failure mechanisms at  $H_r = 0.25$  for reentrant (i) and doubly reentrant (ii) geometries. (C to E) The three failure mechanisms shown in 3D, with associated diagonal cross sections. Critical pressure liquid morphologies are shown in blue, the vapor phase is shown in white, and the interface is indicated with a black solid line. Red regions show how the unstable meniscus evolves upon increasing  $\Delta P$  above  $\Delta P_c$ . (D and E) Under-cap views, highlighting the shapes of the contact lines at the critical pressure. (F) Details of the 3D horizontal (3DD) and 3D diagonal (3DH) capillary bridge models used, showing the inner and outer circumferences (blue) against the system configuration. The 3D illustration compares the simulated liquid-vapor interface (light blue) to the horizontal capillary model (dark blue). Credit: Science Advances, doi: 10.1126/sciadv.aav7328

The scientists first simulated the liquid vapor interface advancing and receding along a single row of surface structures to obtain their respective contact angles and [contact angle hysteresis](#) (CAH, i.e., the difference between advancing and receding contact angles). They arranged the variable dimensions in a square array and observed the hysteresis to be identical for both [reentrant and doubly reentrant geometries](#) (geometries with very low liquid-solid contact fraction). Using the simulation, the scientists observed four dominant receding mechanisms to describe and model them in the present work. Thereafter, using the new models Panter et al. qualitatively tested the [receding models proposed in previous studies](#) to verify their accuracy. They analyzed the energetic changes to obtain the angle at which receding became energetically favorable to form the optimal receding angle.

Unlike simulations of CAH, the second parameter of interest on critical pressure was sensitive to the reentrant or double reentrant surface geometry. The scientists observed three failure mechanisms in the critical pressure study and quantified them as a function of the structural parameters. When they compared quantification in the present work with simulation data, they detected prevailing and widely used critical pressure models introduced in previous studies to be [considerably oversimplified](#). For instance, poor description of the liquid-vapor interface morphology prompted manufactured structures to be many times smaller and mechanically weaker than necessary. By developing a more sophisticated model in the present work, Panter et al. achieved both quantitative accuracy of the critical pressures and successfully modeled the desired complex interfacial morphologies.



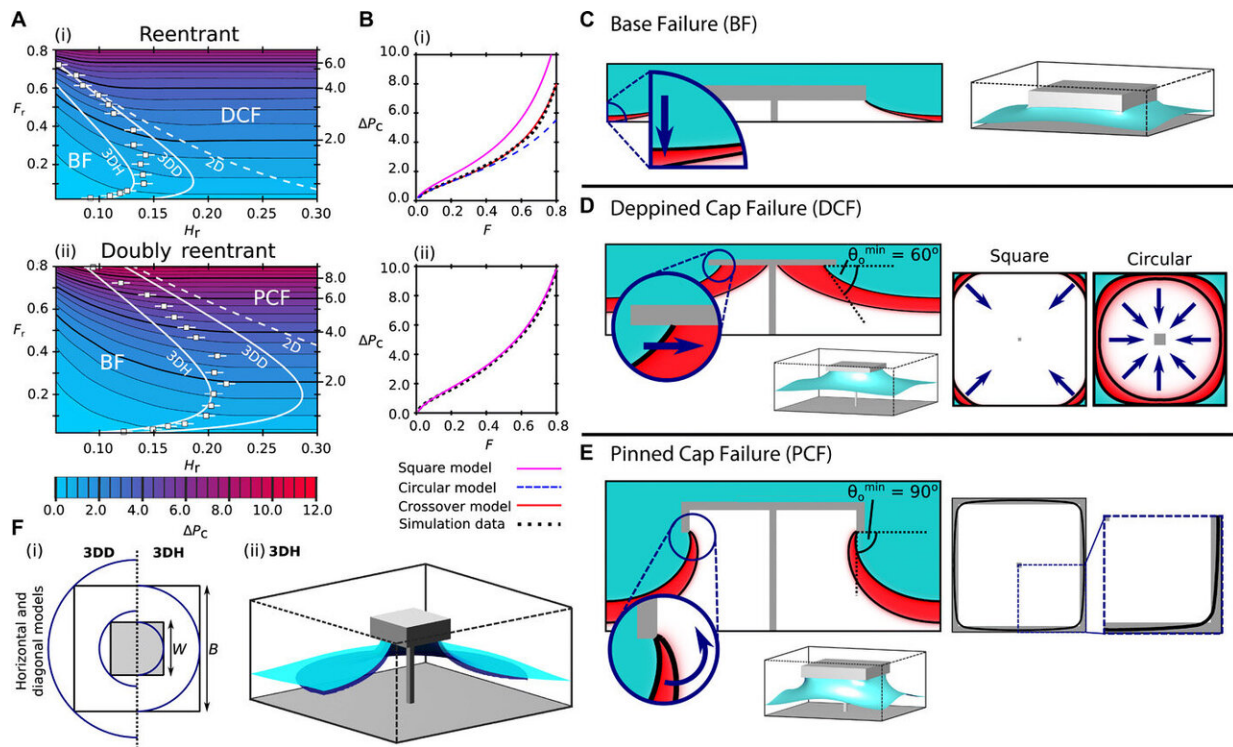
Demonstrating a failure mechanism identified in the study, video shows the base contact (BC) mechanism for a doubly reentrant geometry at  $\theta^\circ = 60^\circ$ . Credit: Science Advances, doi: 10.1126/sciadv.aav7328

When studying the third parameter on minimum energy transition mechanisms, the scientists identified three failure mechanisms. For instance, a surface design failure can be initiated through a broad range of additional perturbations including [flow](#), [vibration](#), [evaporation](#), [condensation](#), [droplet impact](#), changing electrical and magnetic fields or thermal fluctuations [at the nanoscale](#). In real-world applications, failure could be initiated by a combination of perturbations. To fabricate a texture resistant to failure, Panter et al. therefore combined the maximum energy pathway (MEP) to account for a worst case scenario of combined failures. They identified three transition pathways as (1) base contact (BC), (2) pillar contact (PC) and (3) cap contact (CC), then quantified each barrier across the structural parameter space. Thereafter,



they assessed the likeliest mechanism of energy transition for a given [surface](#) geometry.

The scientists then conducted simultaneous optimization of the identified structural features to maximize critical pressure, minimize the energy barrier and maximize the CAH. For this, they performed optimal design of two membranes for applications on water purification and digital microfluidics. Panter et al. also showed that a genetic algorithm could be used to efficiently locate the optimum design in the parameter space and design more complex structures for special wettability applications.



Simultaneous optimization of the three wetting properties for membrane distillation and digital microfluidics applications. (A) (i) 3D contour plot of the membrane distillation scoring function at fixed  $H_r = 0.3$ ,  $Ar = 0.05$ , and  $tr = 0.05$ . Each surface is a surface of constant score. (ii) A 2D slice of the 3D



contour plot at the optimal  $Lr = 0.17$ . Square data points show the initial (white), second (light gray), fifth (dark gray), and final (black) generations of the genetic algorithm, projected onto the 2D plane. (B) Scoring function for the digital microfluidics application, projected onto the  $Hr = 0.3$  plane at fixed  $B = 100 \mu\text{m}$ , also showing the successive generations of the genetic algorithm population. Credit: Science Advances, doi: 10.1126/sciadv.aav7328

In this way, the scientists developed highly versatile computational techniques to study any [mesoscopically structured surface](#) in contact with multiple fluid phases. The multifaceted optimization strategy can be further improved for reliability and scalability to couple with recent advances in fabrication including 3-D printing and lithographic methods to efficiently design real-world superomniphobic surfaces.

**More information:** J. R. Panter et al. Multifaceted design optimization for superomniphobic surfaces, *Science Advances* (2019). [DOI: 10.1126/sciadv.aav7328](https://doi.org/10.1126/sciadv.aav7328)

Arun K Kota et al. The design and applications of superomniphobic surfaces, *NPG Asia Materials* (2014). [DOI: 10.1038/am.2014.34](https://doi.org/10.1038/am.2014.34)

A. Tuteja et al. Robust omniphobic surfaces, *Proceedings of the National Academy of Sciences* (2008). [DOI: 10.1073/pnas.0804872105](https://doi.org/10.1073/pnas.0804872105)

A. Tuteja et al. Designing Superoleophobic Surfaces, *Science* (2007). [DOI: 10.1126/science.1148326](https://doi.org/10.1126/science.1148326)

© 2019 Science X Network

Citation: Multifaceted design optimization for superomniphobic surfaces (2019, June 28) retrieved 25 April 2024 from

<https://phys.org/news/2019-06-multifaceted-optimization-superomniphobic-surfaces.html>

This document is subject to copyright. Apart from any fair dealing for the purpose of private study or research, no part may be reproduced without the written permission. The content is provided for information purposes only.